Original Article

Journal of LOW FREQUENCY NOISE, VIBRATION AND ACTIVE CONTROL

Journal of Low Frequency Noise, Vibration and Active Control
2021, Vol. 40(1) 181–194

DOI: 10.1177/1461348419875056
journals.sagepub.com/home/lfn
SAGE

Dynamic analysis on single-rotor multi-input helicopter main gearbox related with structural parameters

Wei Zhang[1,2] and Luling An[1]

Abstract

Combined with the finite element method and the lumped mass method, the integral node dynamic model of a single-rotor multi-input helicopter main gearbox is established. The influence of shaft parameters on dynamic characteristics is analyzed, and each torsional shaft is regarded as a finite element node to derive the system dynamic equation. In addition, the dynamic model of the meshing pair element is established by lumped mass method, and these elements not only include internal excitations such as time-varying meshing stiffness and transmission error, but also carry the external load. The differential equations of the system are solved by the Fourier series method. The dynamic responses of the converging element and the planetary gear train are obtained. The load-sharing coefficients of these elements are calculated by the influence of the shaft structural parameters. A parameter optimization method is proposed to improve the system load characteristics, which provides a theoretical support for the design of helicopter main transmission system.

Keywords

Single-rotor multi-input helicopter, LMM-FEM mixed modeling, shaft flexibility, load-sharing analysis, parameter optimization

Introduction

The single-rotor multi-input helicopter main gearbox has three identical input branches, converging on a central gear, then the power follows one way to the planetary gear system and the rotor, while the other way to the tail chain. The transmission chain is quite long and it includes many branches, which makes the structure very complicated. In addition, the system is under large load power and severe working conditions. The converging element and the planetary gear train bear dynamic meshing forces in multiple directions, if the load cannot be evenly distributed between the branches, and the carrying capacity will be reduced, resulting in component overload and vibration. Its load-sharing characteristics analysis is for the sake of prolongling system life, reducing vibration and improving system stability, which is regarded as the research hotspot.[1–3] Therefore, the load-sharing analysis is of great significance.

During the past several decades, some significant studies about solving the gearbox dynamic problems have been proposed. About multi-stage gear analysis, Chong et al.[4] proposed a generalized multi-stage gear drives design methodology by integrating the dimensional design and the configuration design processes in a formalized algorithm. Choy et al.[5] presented a three-stage multi-mesh gear transmission systems, and predicted the overall

[1]Jiangsu Key Laboratory of Precision and Micro-manufacturing Technology, Nanjing University of Aeronautics and Astronautics,Nanjing, China
[2]School of Aerospace, Transport & Manufacturing, Cranfield University, Bedford, UK

Corresponding author:
Luling An, Jiangsu Key Laboratory of Precision and Micro-manufacturing Technology, Nanjing University of Aeronautics and Astronautics, Nanjing, 210016, China.
Email: anllme@nuaa.edu.cn

system dynamics by the influence of transmissibility, input speed, rotor imbalances and support. Dzitkowski and Dymarek[6] applied the reduction method based on an active synthesis to obtain a desired mechanical effect by properly selecting the dynamical system properties. Tanaka et al.[7] predicted gear noise from the vibration step to the sound-generation step in a multi-stage gear system, and analyzed the distribution of the sound-pressure around the gearbox and identified the intense noise areas. Thompson et al.[8] applied a basic multi-objective optimization procedure to the design of a three-stage spur gear reduction system, which was subject to identical loading conditions and design criteria.

Regarding load-sharing analysis, Kahraman[9] defined load-sharing in a planetary gear sets by establishing the mathematical model and validated in experimental work under quasi-static conditions. Bodas and Kahraman[10] studied the effect of manufacturing and assembly error on load-sharing behavior in a planetary gear set. Sheng et al.[11,12] presented a new non-linear bending-torsional coupled model for double-row planetary gear set, and studied the influence of planet's eccentricity error and ring gear's supporting stiffness on planetary gear train. Sekar studied load-sharing ratio based on maximum fillet stresses through the asymmetric three-teeth helical model by finite element method, and investigated the influence of gear ratio, transverse contact ratio, top land thickness coefficient and the pinion teeth number.[13] Nevertheless, the influence of shaft parameters on load-sharing behavior has not been adequately analyzed in these researches.

In terms of FEM-LMM mixed gearbox modeling method, Choi et al.[14,15] applied a finite element method with distributed mass for lateral and torsional vibrations, and it was coupled to a lumped mass model describing the axial vibrations, which is the mixed modeling methodology inspiration for this paper.

Stringer presented a comprehensive FEM transmission model by subcomponent, and the multi-node dynamic model of the gearbox was combined with multiple shafts connected by multiple gears of different configurations.[16] However, parameter optimization based on multi-node dynamic modeling has not been captured by these researches.

About auxiliary parameter for nonlinear oscillators, several solving methods such as asymptotic method, homotopy perturbation method, and variational iteration method have been presented by scholars.[17–19] While parameter analysis method for multi-stage gearbox has not been widely applied.

In summary, scholars have focused on the planetary gear train or the single meshing pair; however, the research on the whole helicopter main gearbox has not been widely studied. More importantly, most scholars normally make the derivation of equations in the meshing gear pair, and research on shafts nodes modeling is rarely seen in gearbox dynamic analysis, so it is of great importance for the gearbox design.

Dynamic modeling of multi-node system

The dynamic model of a typical single-rotor multi-input helicopter main gearbox is shown in Figure 1. Figure 1(a) is the system model and Figure 1(b) shows the multi-node model, which is based on the new method.

The main gearbox has a total of three input branches and two output branches (tail chain output branch and rotor output branch).[20] According to Figure 1, there are seven meshing elements (A, B, C, D, E and F) in the system, and the elements F and G are internal and external meshing pairs in planetary system, which contains one sun gear (node 16), six planet gears (nodes 17 to 22) and one carrier (node 23). θ is the rotational degree of freedom (DOF) of each node, and each DOF corresponds to one node. The system's generalized coordinate vector X is

$$X = \left\{\theta_1^{(j)}, \theta_2^{(j)}, \theta_3^{(j)}, \theta_4^{(j)}, \theta_5^{(j)}, \theta_6^{(j)}, \theta_7^{(j)}, \theta_8^{(j)}, \theta_9, \theta_{10}, \theta_{11}, \theta_{12}, \theta_{13}, \theta_{14}\theta_{15}, \theta_{16}, \theta_{17}, \theta_{18}, \theta_{19}, \theta_{20}, \theta_{21}, \theta_{22}, \theta_{23}, \theta_{24}\right\}^T$$

Dynamic modeling of the meshing pairs

For the seven meshing pairs labeled A, B, C, D, E, F, and G in Figure 1, the time-varying meshing stiffness can be expressed in the Fourier series with meshing frequency ω[21]

$$\begin{cases} k(t) = k_m + k_a \sin(\omega t + \beta) \\ k_{\mathrm{sp}i}(t) = k_{\mathrm{m,sp}i} + k_{\mathrm{a,sp}i} \sin(\omega t + \beta_{\mathrm{sp}i}) \\ k_{\mathrm{rp}i}(t) = k_{\mathrm{m,rp}i} + k_{\mathrm{a,rp}i} \sin(\omega t + \beta_{\mathrm{rp}i}) \end{cases} \quad (1)$$

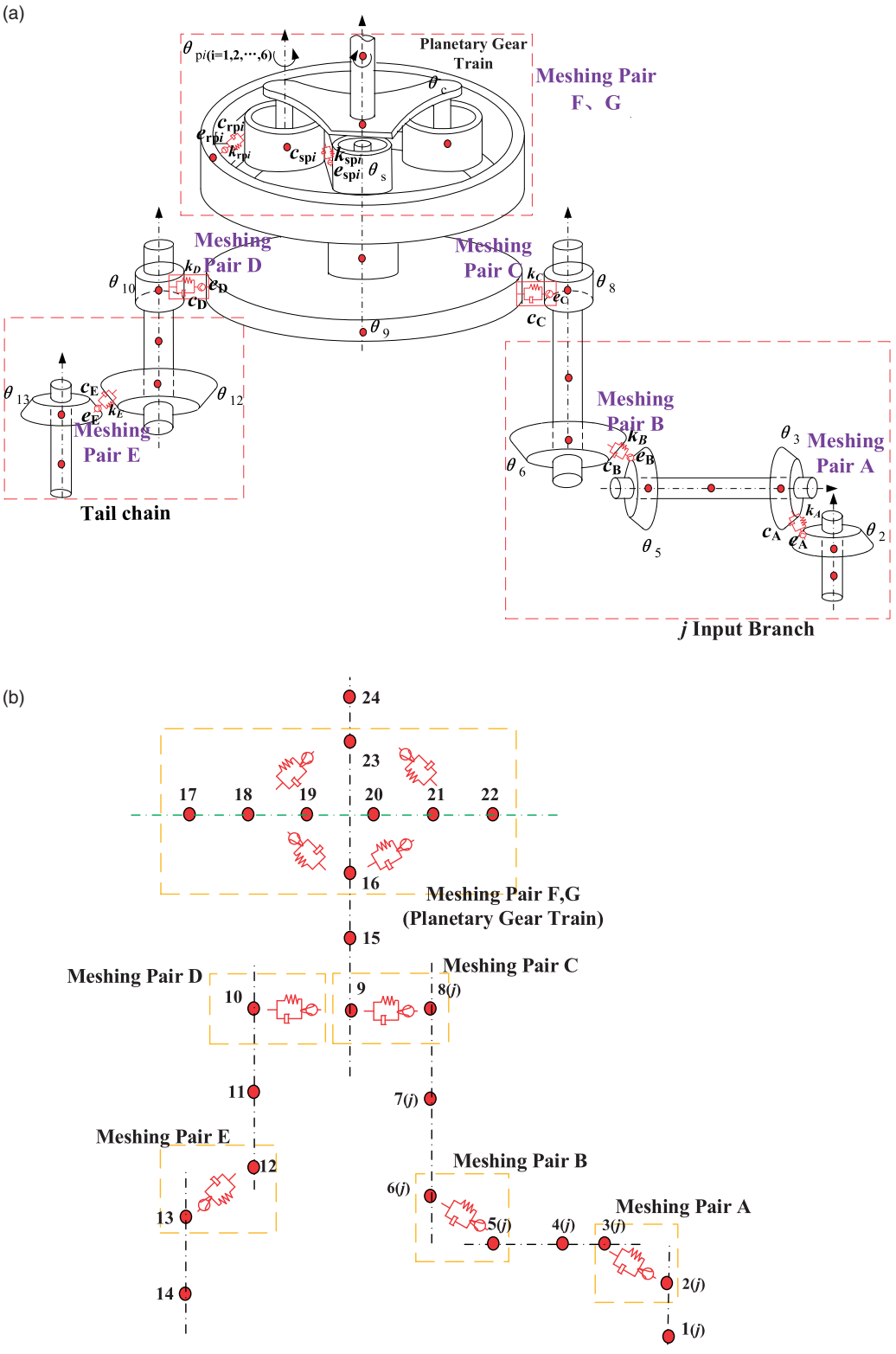

Figure 1. Dynamic model of the multi-node system. (a) Dynamic modeling. (b) Node modeling.

where $k(t)$, $k_{spi}(t)$ and $k_{rpi}(t)$ are time-varying meshing stiffness of each gear pair; k_{m} and k_{a} are the average and maximum variable meshing stiffness; β is the initial phase of meshing stiffness; ω is the fundamental meshing frequency.

Similarly, transmission errors are shown in the same way

$$\begin{cases} e(t) = e_m + e_a\sin(\omega t + \varphi) \\ e_{\mathrm{sp}i}(t) = A_{\mathrm{sp}i}\sin(\omega t + \varphi_{\mathrm{sp}i}) + E_{\mathrm{p}i}\sin(\omega_{pH}t + \varphi_{\mathrm{p}i} + \alpha) + E_{\mathrm{s}}\sin[\omega_{sH}t + \varphi_{\mathrm{s}} - 2\pi(i-1)/N + \alpha] \\ e_{\mathrm{rp}i}(t) = A_{\mathrm{rp}i}\sin(\omega t + \varphi_{\mathrm{rp}i}) + E_{\mathrm{p}i}\sin(\omega_{pH}t + \varphi_{\mathrm{p}i} - \alpha) + E_{\mathrm{r}}\sin[\omega_{\mathrm{r}H}t + \varphi_{\mathrm{r}} - 2\pi(i-1)/N - \alpha] \end{cases} \tag{2}$$

where $e(t)$, $e_{spi}(t)$, $e_{rpi}(t)$ are time-varying transmission error of each gear pair; e_m and e_a are static and dynamic transmission error amplitude; φ is initial phase of transmission error; ω_{pH}, ω_{sH} and ω_{rH} are rotational frequency of planet gear, sun gear and carrier; α is pressure angle; N is the number of planet gear.

The relative displacement along the meshing line $X(t)$ is defined as follows

$$X(t) = \theta_d r_d - \theta_p r_p - e(t) \tag{3}$$

where θ_d and θ_p are rotational response of drive gear and driven gear; r_d and r_p are radius of base circle in drive gear and driven gear.

The dynamic forces of each gear pair $F(t)$ are defined as follows

$$F(t) = k(t)X(t) + c(t)\dot{X}(t) \tag{4}$$

where $c(t)$ is meshing damping; $\dot{X}(t)$ is relative velocity along the meshing line.

Differential equation of multi-node system

According to the above dynamic modeling, the differential equation of the multi-node gearbox model can be deduced through the Newton's law, as is shown below:

Node 1

$$J_1\ddot{\theta}_1{}^{(j)} + G_1\frac{\pi D_1^4}{32l_1}\left(1 - \frac{d^4}{D^4}\right)\theta_1{}^{(j)} = T_{Ej} \tag{5}$$

Node 2

$$J_2\ddot{\theta}_2{}^{(j)} + \left[F_{2\_3}^{p(j)}(t) + F_{2\_3}^{d(j)}(t)\right]r_1 + G_1\frac{\pi D_1^4}{32l_1}\left(1 - \frac{d^4}{D^4}\right)\left(\theta_2{}^{(j)} - \theta_1{}^{(j)}\right) = 0 \tag{6}$$

Node 3

$$J_3\ddot{\theta}_3{}^{(j)} - \left[F_{2\_3}^{p(j)}(t) + F_{2\_3}^{d(j)}(t)\right]r_1 + G_4\frac{\pi D_4^4}{32l_4}\left(1 - \frac{d_4^4}{D_4^4}\right)\left(\theta_3{}^{(j)} - \theta_4{}^{(j)}\right) = 0 \tag{7}$$

Node 4

$$J_4\ddot{\theta}_4{}^{(j)} - G_4\frac{\pi D_4^4}{32l_4}\left(1 - \frac{d_4^4}{D_4^4}\right)\left(\theta_3{}^{(j)} - \theta_4{}^{(j)}\right) + G_4\frac{\pi D_4^4}{32l_4}\left(1 - \frac{d_4^4}{D_4^4}\right)\left(\theta_4{}^{(j)} - \theta_5{}^{(j)}\right) = 0 \tag{8}$$

Node 5

$$J_5\ddot{\theta}_5{}^{(j)} + \left[F_{5\_6}^{p(j)}(t) + F_{5\_6}^{d(j)}(t)\right]r_5 + G_4\frac{\pi D_4^4}{32l_4}\left(1 - \frac{d_4^4}{D_4^4}\right)\left(\theta_5{}^{(j)} - \theta_4{}^{(j)}\right) = 0 \tag{9}$$

Node 6

$$J_6\ddot{\theta}_6{}^{(j)} - \left[F_{5\_6}^{p(j)}(t) + F_{5\_6}^{d(j)}(t)\right]r_6 + G_7\frac{\pi D_7^4}{32l_7}\left(1 - \frac{d_7^4}{D_7^4}\right)\left(\theta_6{}^{(j)} - \theta_7{}^{(j)}\right) = 0 \tag{10}$$

Node 7

$$J_7\ddot{\theta}_7{}^{(j)} - G_7\frac{\pi D_7^4}{32l_7}\left(1 - \frac{d_7^4}{D_7^4}\right)\left(\theta_6{}^{(j)} - \theta_7{}^{(j)}\right) + G_7\frac{\pi D_7^4}{32l_7}\left(1 - \frac{d_7^4}{D_7^4}\right)\left(\theta_7{}^{(j)} - \theta_8{}^{(j)}\right) = 0 \tag{11}$$

Node 8

$$J_8\ddot{\theta}_8{}^{(j)} + \left[F_{8\_9}^{p(j)}(t) + F_{8\_9}^{d(j)}(t)\right]r_8 + G_7\frac{\pi D_7^4}{32l_7}\left(1 - \frac{d_7^4}{D_7^4}\right)\left(\theta_8{}^{(j)} - \theta_7{}^{(j)}\right) = 0 \tag{12}$$

Node 9

$$J_9\ddot{\theta}_9 - \sum_{j=1}^{3}\left[F_{8\_9}^{p(j)}(t) + F_{8\_9}^{d(j)}(t)\right]r_9 + G_{15}\frac{\pi D_{15}^4}{32l_{15}}\left(1 - \frac{d_{15}^4}{D_{15}^4}\right)(\theta_9 - \theta_{15}) + \left[F_{9\_10}^{p}(t) + F_{9\_10}^{d}(t)\right]r_9 = 0 \tag{13}$$

Node 10

$$J_{10}\ddot{\theta}_{10} - \left[F_{9\_10}^{p}(t) + F_{9\_10}^{d}(t)\right]r_{10} + G_{11}\frac{\pi D_{11}^4}{32l_{11}}\left(1 - \frac{d_{11}^4}{D_{11}^4}\right)(\theta_{10} - \theta_{11}) = 0 \tag{14}$$

Node 11

$$J_{11}\ddot{\theta}_{11} + G_{11}\frac{\pi D_{11}^4}{32l_{11}}\left(1 - \frac{d_{11}^4}{D_{11}^4}\right)(\theta_{11} - \theta_{12}) - G_{11}\frac{\pi D_{11}^4}{32l_{11}}\left(1 - \frac{d_{11}^4}{D_{11}^4}\right)(\theta_{10} - \theta_{11}) = 0 \tag{15}$$

Node 12

$$J_{12}\ddot{\theta}_{12} + \left[F_{12\_13}^{p}(t) + F_{12\_13}^{d}(t)\right]r_{12} + G_{11}\frac{\pi D_{11}^4}{32l_{11}}\left(1 - \frac{d_{11}^4}{D_{11}^4}\right)(\theta_{12} - \theta_{11}) = 0 \tag{16}$$

Node 13

$$J_{13}\ddot{\theta}_{13} - \left[F_{12\_13}^{p}(t) + F_{12\_13}^{d}(t)\right]r_{13} + G_{14}\frac{\pi D_{14}^4}{32l_{14}}\left(1 - \frac{d_{14}^4}{D_{14}^4}\right)(\theta_{13} - \theta_{14}) = 0 \tag{17}$$

Node 14

$$J_{14}\ddot{\theta}_{14} + G_{14}\frac{\pi D_{14}^4}{32l_{14}}\left(1 - \frac{d_{14}^4}{D_{14}^4}\right)\theta_{14} = T_t \tag{18}$$

Node 15

$$J_{15}\ddot{\theta}_{15} + G_{15}\frac{\pi D_{15}^4}{32l_{15}}\left(1-\frac{d_{15}^4}{D_{15}^4}\right)(\theta_{15}-\theta_{16}) - G_{15}\frac{\pi D_{15}^4}{32l_{15}}\left(1-\frac{d_{15}^4}{D_{15}^4}\right)(\theta_9-\theta_{15}) = 0 \tag{19}$$

Node 16

$$J_{16}\ddot{\theta}_{16} + \sum_{i=1}^{6}\left[F_{spi}^{p}(t)+F_{spi}^{d}(t)\right]r_{16} + G_{15}\frac{\pi D_{15}^4}{32l_{15}}\left(1-\frac{d_{15}^4}{D_{15}^4}\right)(\theta_{16}-\theta_{15}) = 0 \tag{20}$$

Nodes 17–22 (pi)

$$J_{pi}\ddot{\theta}_{pi} - \left[F_{spi}^{p}(t)+F_{spi}^{d}(t)\right]r_{pi} + \left[F_{cpi}^{p}(t)+F_{cpi}^{d}(t)\right]r_{pi} = 0 \tag{21}$$

Node 23

$$J_{23}\ddot{\theta}_{23} - \sum_{i=1}^{6}\left[F_{cpi}^{p}(t)+F_{cpi}^{d}(t)\right]r_{pi} + G_{24}\frac{\pi D_{24}^4}{32l_{24}}\left(1-\frac{d_{24}^4}{D_{24}^4}\right)(\theta_{23}-\theta_{24}) = 0 \tag{22}$$

Node 24

$$J_{24}\ddot{\theta}_{24} + \sum_{i=1}^{6}\left[F_{cpi}^{p}(t)+F_{cpi}^{d}(t)\right]r_{pi} + G_{24}\frac{\pi D_{24}^4}{32l_{24}}\left(1-\frac{d_{24}^4}{D_{24}^4}\right)(\theta_{24}-\theta_{23}) = -T_r \tag{23}$$

where $T_{\mathrm{E}j}$ is denoted as the torque of engine j (j =1,2,3); d is the internal diameter of the hollow shaft; D is the external diameter of the hollow shaft; l is the shaft length; G is the shear elastic modulus of shaft; T_t is the output torque of tail chain; T_r is the output torque of rotor shaft.

The equations for each DOF could be written as the following matrix – vector form

$$[M]\{\ddot{X}\} + [C]\{\dot{X}\} + [K]\{X\} = \{F\} \tag{24}$$

The excitation $\{F\}$ could be expanded to Fourier series with the fundamental frequency, k^{th} order excitation is

$$F_k = \{A_1\}_k \sin\omega_k t + \{A_2\}_k \cos\omega_k t \tag{25}$$

The excitation would contribute to a certain response

$$\{\Delta x\}_k = \{B_1\}_k \sin\omega_k t + \{B_2\}_k \cos\omega_k t \tag{26}$$

where $\{B_1\}_k$ and $\{B_2\}_k$ could be solved by the following equation

$$\begin{bmatrix} -\omega_k^2[M]+[\bar{K}] & -\omega_k[C] \\ \omega_k[C] & -\omega_k^2[M]+[\bar{K}] \end{bmatrix}\begin{Bmatrix}\{B_1\}_k \\ \{B_2\}_k\end{Bmatrix} = \begin{Bmatrix}\{A_1\}_k \\ \{A_2\}_k\end{Bmatrix} \tag{27}$$

The dynamic response is linear superposition of the result corresponded by each order

$$\{\Delta x(t)\} = \sum_{k=1}^{5}\left\{\{B_1\}_k \sin\omega_k t + \{B_2\}_k \cos\omega_k t\right\} \tag{28}$$

Numerical calculation and dynamic analysis

Parameter setting and response calculation

The node parameters of the system are shown in Table 1. Besides, the system is powered by three engines, the maximum output power of each engine is 1500 kW, output speed is 10,000 r/min. The output power of rotor is 1000 kW, the rotor speed is 300 r/min. The transmission mechanical efficiency is 95%.

In this paper, the Fourier series method is applied to solve the derived differential equations through computational programming, and the time-domain dynamic response of load-sharing-related DOF is obtained and shown in Figure 2. It indicates that the dynamic response exhibits a periodic variation under multi-frequency excitation caused by time-varying meshing stiffness and various errors. The three input branches are important components in single-rotor multi-input helicopter main gearbox, they are in the same structure but different excitation, and as a result, they show distinct response amplitude.

By comparison, it can be seen that the dynamic response of meshing element E has the maximum amplitude due to the load of tail chain. In addition, under the converging influence of the three-input branches, the magnitude of the response of the converging element (composed of the meshing pair C and D) is also relatively large, and thus needs further analysis. Regarding the responses in the internal and external meshing pair (element F and G), planetary gear 1 is greater than other planetary gears due to its largest transmission and manufacturing error.

Load-sharing coefficient calculation

Due to the manufacturing error, installation error, gear wear and other factors in the planetary gear train, the load distribution on each gear pair is inconsistent. The converging element also has inconsistent load distribution due to the multiple convergences of input branches. The basic assumption is that some factors like transmission error and phase difference are intrinsically existing. A method is proposed by changing the thickness and length of the shaft, and the load-sharing characteristics can be improved, thus providing technical support for the shaft parameter design.

The load-sharing coefficient b is defined as the ratio of the maximum dynamic meshing force to the mean value in separate branch

$$b(t) = \frac{N(P_k)_{\max}}{\sum_{k=1}^{N} (P_k)_{\max}} \tag{29}$$

where P_k is the dynamic meshing force of k branch; N is the number of branches.

According to dynamic response and time-varying meshing stiffness, the meshing force could be calculated, and then the load-sharing coefficients of the converging element and planetary gear systems could be computed, which are depicted in Figure 3. The load-sharing coefficients also show the periodic variation under multi-frequency excitation. The value of converging element is larger than that of the planetary gear system due to the complex coupling impact of three input branches and tail chain. In terms of planetary gear systems, the external meshing coefficient is larger than that of internal pair.

Analysis on load-sharing coefficient influenced by shaft wall thickness

The wall thickness is characterized by the ratio of the external diameter to the internal diameter of the hollow shaft, which is symbolized as α. In this case study, $0.6 \leq \alpha \leq 0.9$ is originally set, and the influence of the thickness on load-sharing coefficient at this interval is investigated. By changing the value of α in each shaft, the maximum load-sharing coefficient is calculated without changing other parameters, and the result is shown in Figure 4.

Figure 4(a) shows that the load-sharing coefficient of converging element is the lowest (1.032) when α_1 is 0.57. If α_1 is greater than 0.7, the load-sharing coefficient of internal meshing in the planetary gear is reduced, but the change is not significant. The load-sharing coefficient of external meshing does not change with α_1.

Figure 4(b) demonstrates that when α_4 is greater than 0.8, the load-sharing coefficient of the converging element decreases more significantly, while the other two stages do not change apparently. Therefore, the thin-walled characteristics of Node 4 can improve the system stability.

Similarly, from Figure 4(c) to (e), it can be seen that when α_7 is equal to 0.81, α_{11} is equal to 0.76, and α_{14} is equal to 0.9, the load-sharing coefficient of the converging element can also be reduced. Among them, the

Table 1. Single-rotor multi-input helicopter main gearbox node parameters.

Element	Node	Tooth number	Module (mm)	Face width (m)	Transmission error (μm)	Initial phase of transmission error	Initial phase of meshing stiffness	Shaft *D*/*d* (m)	Shaft length (m)
Shaft element	1(*i*)	–	–	–	–	–	–	0.04/0.03	0.8
Meshing element A	2(*i*)	28	5	0.04	12; 18; 14	$\pi/3$; $\pi/9$; $4\pi/3$	0; 0; 0	–	–
	3(*i*)	86	5	0.04	12; 18; 14	$\pi/3$; $\pi/9$; $4\pi/3$	0; 0; 0	–	–
Shaft element	4(*i*)	–	–	–	–	–	–	0.06/0.05	1.6
Meshing element B	5(*i*)	38	4.5	0.35	22; 17; 15	$-\pi/9$; $-4\pi/3$; 0	$\pi/3$; $\pi/9$; $\pi/3$	–	–
	6(*i*)	88	4.5	0.35	22; 17; 15	$-\pi/9$; $-4\pi/3$; 0	$\pi/3$; $\pi/9$; $-\pi/3$	–	–
Shaft element	7(*i*)	–	–	–	–	–	–	0.06/0.04	2.2
Meshing element C, D	8(*i*)	65	3	0.42	8; 12; 10	$-\pi$; 0; $-\pi/6$	0; 0; 0	–	–
	9	144	3	0.42	8; 12; 10	$-\pi$; 0; $-\pi/6$	0; 0; 0	–	–
	10	70	3	0.42	10	$-\pi/6$	0	–	–
Shaft element	11	–	–	–	–	–	–	0.04/0.03	1.4
Meshing element E	12	40	3.5	0.47	12	$\pi/9$	0	–	–
	13	70	3.5	0.47	12	$\pi/9$	0	–	–
Shaft element	14	–	–	–	–	—	—	0.04/0.03	1.1
Shaft element	15	–	–	–	–	—	—	0.14/0.11	0.8
Meshing element F, G	16	68	5	0.4	13; 8; 6; 8; 12; 5	$-4\pi/3$; $\pi/9$; $-\pi/7$; $-\pi/9$; $\pi/3$; $-\pi/9$	π; 0; $4\pi/7$; 0; $-\pi/3$; 0	–	–
	17	37	5	0.4	13; 8	$-4\pi/3$; $-\pi$	π; $-\pi/3$	–	–
	18	37	5	0.4	8; 9	$\pi/9$; 0	0; $4\pi/3$	–	–
	19	37	5	0.4	6; 7	$-\pi/7$; $4\pi/3$	$4\pi/7$; $-\pi$	–	–
	20	37	5	0.4	8; 6	$-\pi/9$; $-\pi/9$	0; $-4\pi/3$	–	–
	21	37	5	0.4	12; 6	$\pi/3$; $\pi/9$	$-\pi/3$; 0	–	–
	22	37	5	0.4	5; 8	$-\pi/9$; $-5\pi/3$	0; π	–	–
	23	142	5	0.4	8; 9; 7 6; 6; 8	$-\pi$;0; $4\pi/3$;$-\pi/9$; $\pi/9$;$-5\pi/3$	$-\pi/3$; $4\pi/3$; $-\pi$;$4\pi/3$; 0;π	–	–
Shaft element	24	–	–	–	–	–	–	0.12/0.09	2.0

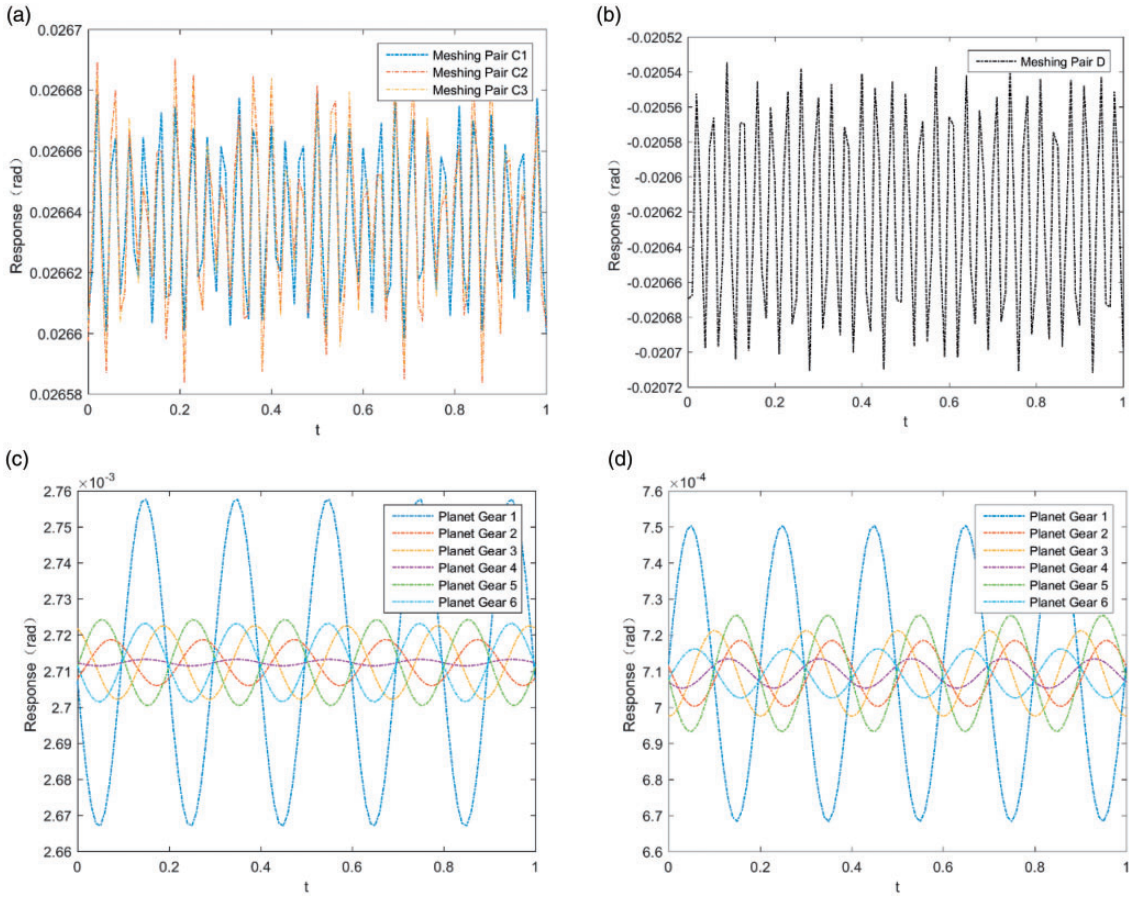

Figure 2. Time-domain dynamic response in confluent stage. (a) Meshing pair C. (b) Meshing pair D. (c) Meshing pair F. (d) Meshing pair G.

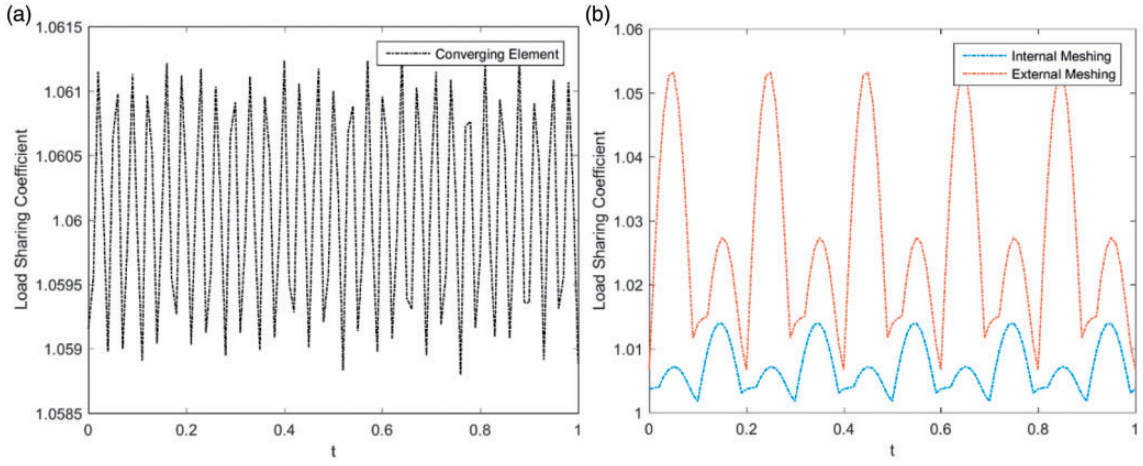

Figure 3. Time domain of load-sharing coefficient in the system. (a) Converging element. (b) Planetary gear train.

influence of the shaft diameter ratio of Node 7 is the most obvious, and therefore it is the key shaft of the load-sharing characteristics of this element.

According to Figure 4(f) and (g), the wall thickness of Node 15 and Node 24 are key factors in internal and external meshing pairs, and when the diameter ratios are equal to 0.6, the system load-sharing characteristics tend to be better.

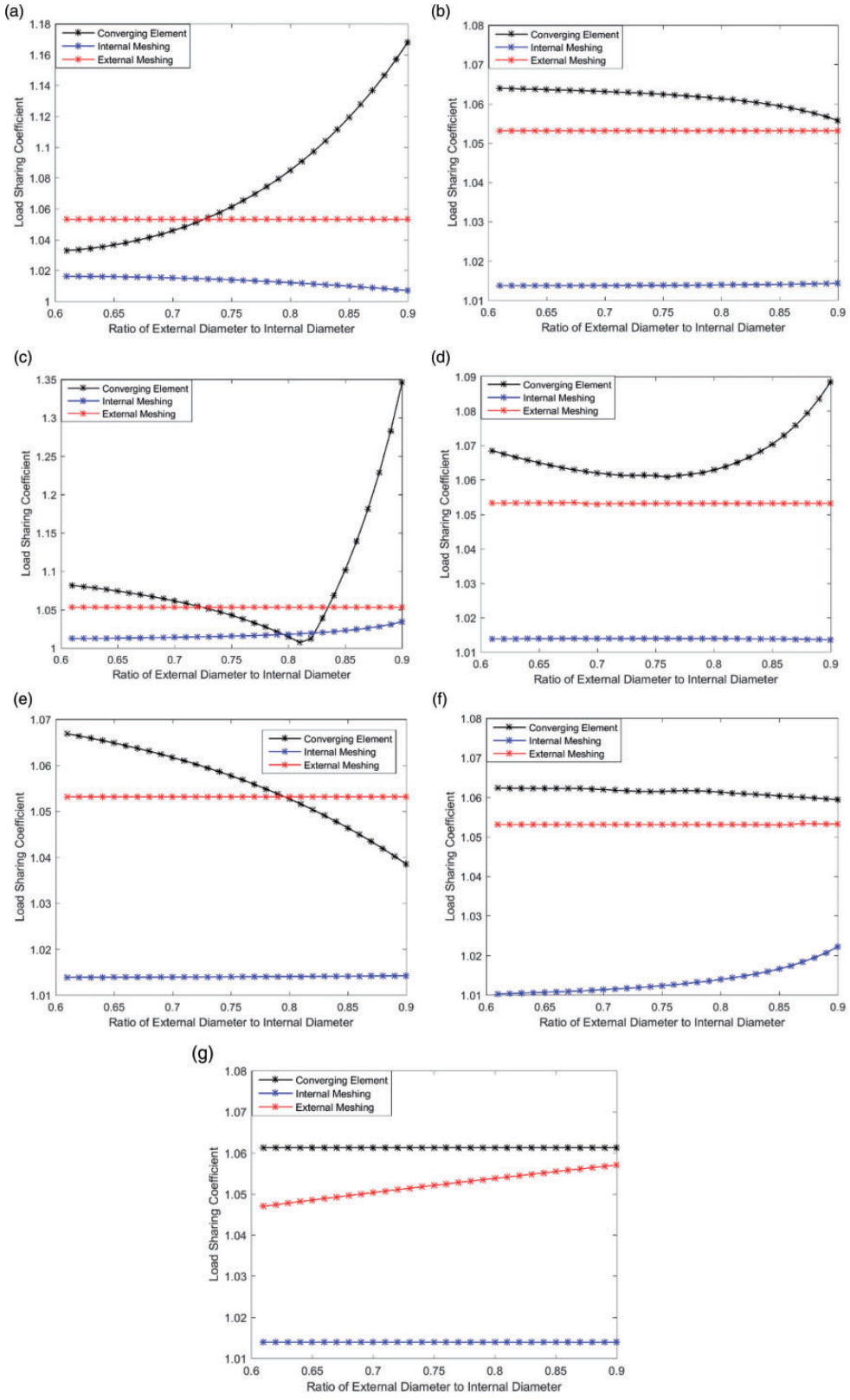

Figure 4. Load-sharing coefficient influenced by wall thickness. (a) Node 1. (b) Node 4. (c) Node 7. (d) Node 11. (e) Node 14. (f) Node 15. (g) Node 24.

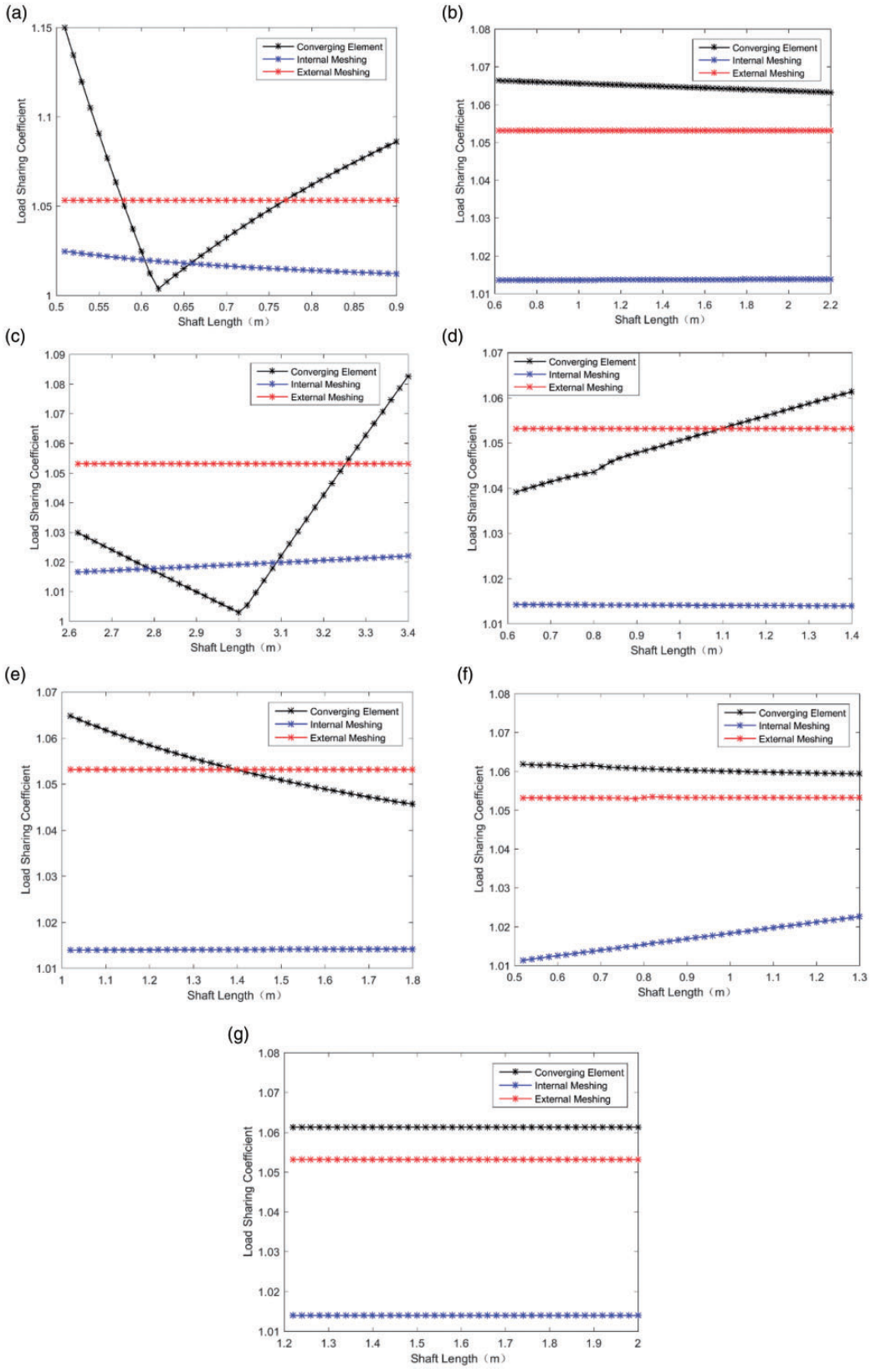

Figure 5. Load-sharing coefficient influenced by shaft length. (a) Node 1. (b) Node 4. (c) Node 7. (d) Node 11. (e) Node 14. (f) Node 15. (g) Node 24.

Table 2. Parameter optimization of the hollow shaft.

	α_1	α_4	α_7	α_{11}	α_{14}	α_{15}	α_{24}
Parameter							
Original group	0.75	0.8	0.7	0.73	0.7	0.8	0.78
Improved group	0.57	0.9	0.81	0.76	0.9	0.6	0.6
	l_1	l_4	l_7	l_{11}	l_{14}	l_{15}	l_{24}
Original group	0.8	1.6	2.2	1.4	1.1	0.8	2
Improved group	0.62	2.2	3	0.6	1.8	0.5	2

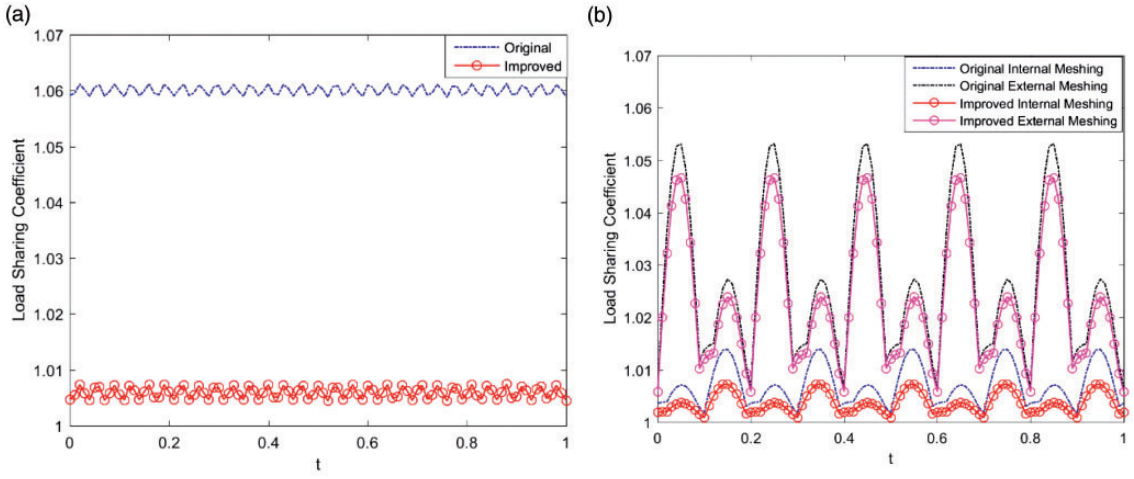

Figure 6. Load-sharing optimization. (a) The converging element. (b) The planetary gear train.

Table 3. Shaft node parameter optimization.

	Converging element	Internal meshing	External meshing
Original group	1.0613	1.014	1.053
Improved group	1.0074	1.0037	1.047
Optimization effect	−5.1%	−1.01%	−0.98%

Analysis on load-sharing coefficient influenced by shaft length

The load-sharing coefficient is calculated by changing the shaft length of each node within the allowable range, without changing other parameters, and the result is shown in Figure 5.

In Figure 5(a), it can be concluded that l_1 is the most effective parameter in improving the load-sharing characteristics of the converging element. When l_1 is equal to 0.62 m, it is the turning point of the figure, which can reduce the load-sharing coefficient to 1.01. Similarly, it could be noted from Figure 5(b) to (e) that when l_4 is 2.2 m, l_7 is 3.0 m, l_{11} is 0.6 m, and l_{14} is 1.8 m, the load-sharing coefficient could be reduced as well, while the other two elements are not affected. From Figure 5(f), the Node 15 is still the key shaft of the load-sharing characteristics in the planetary gear system. When l_{15} is short, the system internal meshing load-sharing characteristics tend to be better. The change in the length of the Node 24 does not affect the load-sharing coefficients of the three elements.

Structural parameter optimization based on load-sharing coefficient analysis

Based on the above analysis, according to the relationship between the shaft parameters and the load-sharing coefficient at each stage, the improved parameters at the shaft node are obtained, and thus the original parameters

are replaced with the improved, as is shown in Table 2. The load-sharing coefficients of the converging element and planetary gear train are recalculated, and the improved effect is shown in Figure 6 and Table 3. As indicated from the figure and the table, the waveform and phase of both elements do not make a change, but the load-sharing coefficients have been significantly reduced. Since Node 1, Node 4, Node 7, Node 11 and Node 14 can effectively improve the load-sharing characteristics in converging element, the coefficient of this element is reduced by 5.1%, which is more effective than that of the other two elements. There are not many parameters affecting the load-sharing coefficient of the planetary gear system, but the internal and external meshing pairs are still improved by 1.01% and 0.98%, respectively.

In summary, a parameter optimization method to improve the system load-sharing characteristics is provided for the gearbox design.

Conclusion

Based on the load-sharing characteristics analysis, this paper proposes a structural parameter optimization method for single-rotor multi-input helicopter main gearbox. By establishing the multi-node dynamic model, deducing coupling differential equations, and analyzing load-sharing coefficients of three stages, the influence law of shaft thickness and shaft length is obtained. The results could draw the following conclusions:

1. The dynamic response shows a periodic variation under the multi-frequency excitation, and meshing elements C, D, and E have relatively larger response.
2. Node 7, Node 15 and Node 24 are key nodes regarding load-sharing characteristics of the converging element, internal and external meshing elements, respectively. By changing the wall thickness (shaft diameter ratio α), the load-sharing coefficient could be reduced according to the corresponding influence law.
3. The length parameter of Node 1 has the most obvious effect on the improvement of the load-sharing characteristics in the converging element; the length parameter of Node 15 is the key parameter related to the planetary gear element; Length of the Node 24 does not affect the load-sharing coefficients in these elements.
4. By the structural parameter optimization method, the load-sharing coefficient of the original group can be reduced by 5.1%, and the load-sharing characteristics of internal and external meshing pairs can be improved by 1.01% and 0.98%, respectively.

Acknowledgements

The authors gratefully acknowledge the help of Professor Rupeng Zhu and Dr Yuan Chen for the guidance of the final revision.

Declaration of conflicting interests

The author(s) declared no potential conflicts of interest with respect to the research, authorship, and/or publication of this article.

Funding

The author(s) disclosed receipt of the following financial support for the research, authorship, and/or publication of this article: The work described in this paper is fully supported by Jiangsu Key Laboratory of Precision and Micro-manufacturing Technology Foundation (Grant No.ZAA1400105); Aeronautical Science Foundation of China (Grant No.20161852018); Innovation Fund of National Commercial Aircraft Manufacturing Engineering Technology (Grant No.SAMC13-JS-13-021).

ORCID iD

Wei Zhang https://orcid.org/0000-0002-8862-9772

References

1. Kahraman A. Load sharing characteristics of planetary transmissions. *Mech Mach Theory* 1994; 29: 1151–1165.
2. Li M, Xie L and Ding L. Load sharing analysis and reliability prediction for planetary gear train of helicopter. *Mech Mach Theory* 2017; 115: 97–113.
3. Ren F, Qin D, Lim TC, et al. Study on dynamic characteristics and load sharing of a herringbone planetary gear with manufacturing errors. *Int J Precis Eng Manuf* 2014; 15: 1925–1934.

4. Chong TH, Bae I and Park GJ. A new and generalized methodology to design multi-stage gear drives by integrating the dimensional and the configuration design process. *Mech Mach Theory* 2002; 37: 295–310.
5. Choy FK, Tu YK, Savage M, et al. Vibration signature and modal analysis of multi-stage gear transmission. *J Franklin Inst* 1991; 328: 281–298.
6. Dzitkowski T and Dymarek A. Active reduction of identified machine drive system vibrations in the form of multi-stage gear units. *Mechanics* 2014; 20: 183–189.
7. Tanaka E, Houjoh H, Mutoh D, et al. Vibration and sound-radiation analysis for designing a low-noise gearbox with a multi-stage helical gear system. *JSME Int J Ser C* 2003; 46: 1178–1185.
8. Thompson DF, Gupta S and Shukla A. Tradeoff analysis in minimum volume design of multi-stage spur gear reduction units. *Mech Mach Theory* 2000; 35: 609–627.
9. Kahraman A. Static load sharing characteristics of transmission planetary gear sets: model and experiment. *SAE Transac* 1999; 108: 1954–1963.
10. Bodas A and Kahraman A. Influence of carrier and gear manufacturing errors on the static load sharing behavior of planetary gear sets. *JSME Int J Ser C* 2004; 47: 908–915.
11. Sheng DP, Zhu RP, Jin GH, et al. Dynamic load sharing characteristics and sun gear radial orbits of double-row planetary gear train. *J Cent South Univ* 2015; 22: 3806–3816.
12. Sheng DP, Zhu RP, Jin GH, et al. Dynamic load sharing behavior of transverse-torsional coupled planetary gear train with multiple clearances. *J Cent South Univ* 2015; 22: 2521–2532.
13. Sekar RP and Muthuveerappan G. Load sharing based maximum fillet stress analysis of asymmetric helical gears designed through direct design – A parametric study. *Mech Mach Theory* 2014; 80: 84–102.
14. Choi SH, Glienicke J, Han DC, et al. Dynamic gear loads due to coupled lateral, torsional and axial vibrations in a helical geared system. *J Vib Acoust* 1999; 121: 141–148.
15. Choi SH, Pierre C and Ulsoy AG. Consistent modeling of rotating Timoshenko shafts subject to axial loads. *J Vib Acoust* 1992; 114: 249–259.
16. Stringer DB, Sheth PN and Allaire PE. A new helicopter transmission model for condition-based maintenance technologies using first principles. In: *45th AIAA/ASME/SAE/ASEE joint propulsion conference & exhibit*, Cleveland, Ohio, USA, September 2009, p.4887.
17. He JH. Some asymptotic methods for strongly nonlinear equations. *Int J Mod Phys B* 2006; 20: 1141–1199.
18. He JH. Recent development of the homotopy perturbation method. *Topologic Meth Nonlinear Anal* 2008; 31: 205–209.
19. Ahmad H. Variational iteration method with an auxiliary parameter for solving differential equations of the fifth order. *Nonlinear Sci Lett A* 2018; 9: 27–35.
20. Bianchi A and Rossi S. Modeling and finite element analysis of a complex helicopter transmission including housing. *Shafts Gears* 1997: 61–76.
21. Chen Y, Zhu RP, Xiong YP, et al. Analysis on natural characteristics of four-stage main transmission system in three-engine helicopter. *Vibroeng Proc* 2017; 12: 19–23.

2019-09-26

Dynamic analysis on single-rotor multi-input helicopter main gearbox related with structural parameters

Zhang, Wei

Sage

Zhang W, An L. (2019) Dynamic analysis on single-rotor multi-input helicopter main gearbox related with structural parameters. Journal of Low Frequency Noise, Vibration and Active Control, Volume 40, Issue 1, March 2021, pp. 181-194

https://doi.org/10.1177/1461348419875056